Mahmud Hossain[1,*], Christian Telke[2], Anwar Abdkader[1], Maria Sparing[3], Tilo Espenhahn[3], Ruben Hühne[3], Chokri Cherif[1], Michael Beitelschmidt[2]

Mathematical Modelling of Dynamic Yarn Path Considering the Balloon Control Ring and Yarn Elasticity in the Ring Spinning Process Based on the Superconducting Bearing Twisting Element

DOI: 10.5604/01.3001.0012.2528

[1] **Technische Universität Dresden, Faculty of Mechanical Engineering,** Hohe Straße 6, Dresden-01069, Germany
* e-mail: mahmud.hossain@tu-dresden.de

[2] **Technische Universität Dresden, Institute of Solid Mechanics, Chair of Dynamics and Mechanism Design,** Marschnerstraße 30, 01307 Dresden, Germany

[3] **Institute for Metallic Materials, IFW Dresden,** Helmholtzstraße 20, 01069 Dresden, Germany

Abstract
The productivity of the conventional ring spinning process is currently limited by the frictional heat that occurs in the ring/traveler twisting system. In the framework of a fundamental research project from the German Research Foundation (DFG), the levitation principle of superconducting magnetic bearing (SMB) was implemented as a twisting element in order to eliminate the frictional problem and thus aim, at least, to double the productivity. A mathematical model of the dynamic yarn path has already been presented considering the friction free SMB system up to an angular spindle speed of 25.000 r.p.m. In this paper, the existing theoretical model, which was developed up to 25.000 r.p.m, was further modified considering the balloon control ring and yarn elasticity at a higher angular spindle speed, such as 50.000 r.p.m. The model was solved numerically using the Runge-Kutta method. With this model, it is possible to estimate the yarn tension distribution and balloon form considering the above-mentioned parameters. The model established was further validated by comparing the yarn tension and balloon forms predicted with measured ones up to an angular spindle speed of 15.000 r.p.m in a ring spinning tester based on superconducting magnetic bearing.

Key words: *mathematical modelling, balloon control ring, yarn elasticity, yarn tension, balloon form, ring spinning, superconducting magnetic bearing.*

Introduction

According to the principle of the superconducting magnetic bearing (SMB) system, a permanent magnet (PM) ring levitates over the superconductor and rotates unlike the traveler of the existing twisting system to impart twist to the yarn. Thus the SMB twisting system replaces the existing ring/traveler system and eliminates frictional heat between the ring and traveler [1-5]. However, another limitation of ring spinning is the yarn tension, which increases together with the angular spindle speed. In this case, the balloon control rings (BCRs) help to restrict the rotating balloon and reduce the yarn tension to some extent during the ring spinning process at higher speeds. Thus the implementation of one or more BCRs should improve stability in the SMB ring spinning process. Moreover the non-linear behaviour of yarn and the harmonic as well as non-harmonic oscillation of the yarn and SMB system play an important role in the dynamic yarn path at a higher angular spindle speed, such as 50,000 r.p.m. Thus the aims of the mathematical modelling of the yarn path presented in this paper are as follows:

- Mathematical formulation of the yarn dynamics considering an additional BCR and linear yarn elasticity up to an angular spindle speed of 50.000 r.p.m.
- Determination of yarn tension distribution in different regions of the yarn path with respect to the angular spindle speed
- Investigation of the influence of BCR and yarn elasticity on yarn tension and balloon geometry.

State of mathematical modelling

There are different theoretical models of the dynamic yarn path in the ring spinning process [6-10]. Fraser [10] considered the balloon control ring (BCR) as a point constraint in the balloon that exerts a point force on the yarn. Later on he [11] assumed that the motion of the yarn slides over the toroidal surface of the control ring. He proved that the BCR lowers the yarn tension in the balloons and helps to stabilise them as well. Tang [12] examined the effect on yarn tension and balloon flutter stability with respect to different diameters and locations of BCR. He estimated that the maximum yarn tension can be reduced by up to two-thirds with the use of a single BCR with optimal ring size and position. The purpose of the existing models is to analyse the yarn tension distribution and balloon form in the ring spinning process based on the ring/traveler twisting system. In the quasi-stationary model, a non-dimensional equation of motion of yarn has been established to represent the physical influences in a more general way. As the differential equations are extremely non-linear, all the parameters have not been considered in those models in order to solve the problem without complexity. Moreover these models have described the effect of the BCR in a dimensionless form in the conventional ring spinning process. In [13-14], the dimensioned equation has been taken into account and solved numerically using the Runge-Kutta method considering different angular spindle speeds. Sensitivity analysis of the model developed results in a valid solution space for the numerical solution. The model has been further optimised with the shooting method to minimise residual error in the MATLAB program. Thus the yarn tension and balloon form are calculated in the conventional ring spinning process. The model with the dimensioned equation has been further developed and validated considering the dynamics of the SMB system, replacing the conventional ring/traveler twisting element [14]. Moreover a theoretical model has been established in aquasi-stationary state considering the linear elasticity for different materials in order to simulate the balloon form and

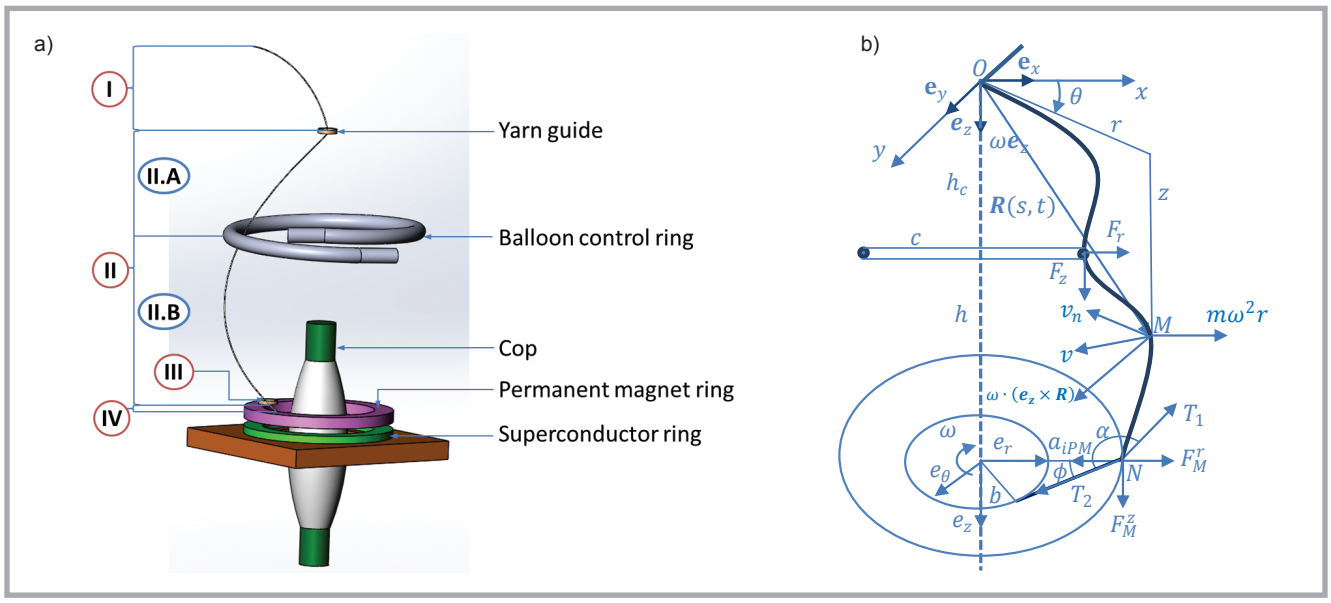

Figure 1. *Definition of: a) yarn path and b) coordinate system in region II considering the balloon control ring. Region I – from the clamping point of the delivery rollers to the yarn guide, Region II – from the yarn guide to the PM ring (IIA: between yarn guide and BCR and IIB: between BCR and PM ring), Region III – yarn passage through the yarn guide of the PM ring, and Region IV – from the PM ring to the winding-point on the cop.*

predict yarn tension under given conditions for a small strain (less than 3.7%), which helps to reduce the yarn breakage in ring spinning [15]. According to this model, yarn tension is decreased by elasticity, which causes a slight increase in the balloon radius.

However, the balloon control ring (BCR) and yarn elasticity have not been considered in the theoretical model of the SMB ring spinning process. Therefore the model [12] has been further developed considering the influence of the BCR and elasticity of yarn in the SMB based ring spinning process, especially at a higher angular spindle speed, such as 50.000 r.p.m.

Assumptions of the model

In the mathematical formulation of the dynamic yarn path, the yarn is considered as a one-dimensional continuum with a homogeneous and circular cross section. The other important assumptions and limitations of the model presented are as follows:

- The effect of the balloon control ring is considered.
- The elasticity of yarn is considered.
- The friction between the yarn and yarn guide attached to the permanent magnet (PM) ring in the SMB ring spinning process is measured and considered in the simulation.
- The friction between the yarn and BCR is neglected.
- The influences of the centrifugal force and Coriolis force are considered.

Theoretical model considering the balloon control ring and yarn elasticity

Definition of the coordinate system and mathematical formulation

The yarn path from delivery rollers up to the winding point of the cop can be segmented into four regions: region I – from the clamping point of delivery rollers to the yarn guide, region II – from the yarn guide to the PM ring (1st sub region: between the yarn guide and BCR and 2nd sub region: between the BCR and PM ring), region III – yarn passage through the yarn guide of the PM ring and region IV – from the PM ring to the winding-point on the cop (***Figure 1.a***). As the yarn path in region I is nearly straight, no dynamic force occurs in this region. Hence the coordinate system $r(s)$, $\theta(s)$, $z(s)$ with corresponding unit vectors e_r, e_θ, e_z is defined in the yarn path in region II i.e. the yarn path between the yarn guide and SMB system, as shown in ***Figure 1.b***. The BCR in this coordinate system is assumed to be a point constraint on the yarn in the balloon that exerts a point force on the yarn at distance $s = s_c$ ($z(s_c) = h_c$) along the thread line from the guide eye. h_c is the distance between the yarn guide and BCR.

As shown in ***Figure 1.b***, if a material point M is defined as the position vector $R(s, t) = re_r + ze_z$ in region II, an ***Equation (1)*** of yarn dynamics can be formulated according to the well-known equation of motion [10].

Where, m is the yarn mass in g/km, ω_{PM} the angular velocity of the PM ring, $\mathfrak{D}$ the differential operator, T the yarn tension at M, F the air drag force per unit length, and F_c is the point force of the BCR exerted on the yarn.

The ***Equation (2)*** of motion is further applied in a dimensioned form based on [6].

Where, v is the velocity of the yarn at the delivery rollers.

$$m\{\mathfrak{D}^2 R + 2\omega_{PM} e_z \times \mathfrak{D}R + \omega_{PM}^2 e_z \times (\boldsymbol{e_z} \times R)\} = \frac{\partial}{\partial s}\left(T\frac{\partial}{\partial s}R\right) + F + F_c \quad (1)$$

$$m\left\{v^2\frac{\mathrm{d}^2R}{\mathrm{d}s^2} + 2\omega_{PM} v e_z \times \frac{\mathrm{d}R}{\mathrm{d}s} + \omega_{PM}^2 e_z \times (e_z \times R)\right\} = T'\frac{\mathrm{d}R}{\mathrm{d}s} + T\frac{\mathrm{d}^2R}{\mathrm{d}s^2} + F + F_c \quad (2)$$

Equations (1) and (2).

Mathematical formulation considering the elasticity of the yarn

The definition of strain is consistent with the usual definition of strain in linear-elasticity theory as the ratio of elongation with respect to the original length. If E is Young's modulus, T is the tension at point M, and A is the cross-sectional area of unstretched yarn, which leads to the following ***Equation (3)***:

$$\varepsilon = \frac{\partial l}{\partial s} - 1 = \frac{T}{AE} \tag{3}$$

If the yarn strain ε is along the yarn length, the difference in the position vector at point M can be expressed as ***Equation (4)***:

$$dR = ds(1+\varepsilon) \tag{4}$$

Thus replacing the inextensibility assumption can be formed as follows [15]:

$$\frac{\partial R}{\partial s} \cdot \frac{\partial R}{\partial s} = (1+\varepsilon)^2 \tag{5}$$

The elasticity of the material is dependent on its type , which influences the yarn tension distribution as well. Considering the elasticity of yarn, the unit tangent vector to the yarn path in ***Equation (1)*** will be $\frac{\partial R}{\partial s}/(1+\varepsilon)$. Thus ***Equation (1)*** is modified considering the yarn elasticity and balloon control ring as follows ***Equation (6)***.

Where, $\mathfrak{D}^2 R$ denotes the yarn acceleration, $2\omega_{PM} e_z \times \mathfrak{D}R$ the Coriolis acceleration and $\omega_{PM}^2 e_z \times (e_z \times R)$ the yarn centrifugal acceleration relating to the rotating reference frame.

The drag force per yarn length F can be expressed as follows [10] ***Equation (7)***.

D_n describes the air drag constant, v_n the normal component of the yarn velocity at point M, ρ the air density in kg/m^3, d the yarn diameter in m, c_d the air drag coefficient, and ρ_m is the density of yarn in kg/m^3.

The component equations of ***Equation (6)*** are described as follows ***Equations (8), (9), (10)***.

Where, T_0 is the yarn tension at the yarn guide, μ_c the co-efficient of friction between the yarn and balloon control ring, and F_r and F_z are the component forces that are exerted from the control ring on the yarn.

Boundary conditions of the modelling

The boundary conditionsvat the upper yarn guide as illustrated in ***Figure 1.b*** are:

$$r(0) = 10^{-3}\,\mathrm{m},\ \theta(0) = 0,\ z(0) = 0. \tag{11}$$

The boundary conditions due to the integration of the BCR are the geometrical constraints at $s = s_c$:

$$r(s_c) = c, z(s_c) = h_c \tag{12}$$

where, c is the radius of the BCR, and h_c is the vertical distance between the upper yarn guide and BCR. The first boundary conditions at the yarn guide of the PM ring, N (***Figure 1.b***) are

$$r(s_l) = a_{iPM},\ z(s_l) = h \tag{13}$$

s_l describes the length of the yarn between the upper yarn guide and the yarn guide of the PM ring at N, and h is the balloon height (***Figure 1.b***).

The 2nd boundary condition at the yarn guide of the PM ring i.e. in region III, is defined from the ***Equation (14)*** of motion of the PM ring:

$$T_1[g\sin\phi - a_{iPM}\theta'(s_l)]a_{iPM} = d_R\omega_{PM} \tag{14}$$

T_1 is the yarn tension at the yarn guide of the PM ring on the balloon side, $g\,(= e^{\mu_y \alpha})$ the frictional parameter between the yarn and yarn guide of the PM ring, d_R the damping constant of rotation of the rotating PM ring and $()' \equiv d()/ds$. The yarn tension at the yarn guide of the PM ring on the cop side T_2 (***Figure 1.b***) i.e. in region IV is estimated by Euler equation as follows

$$T_2 = T_1 \cdot e^{\mu_y \alpha} \tag{15}$$

where μ_y is the frictional co-efficient between the yarn and yarn guide of the PM ring, and α is the angle, shown in ***Figure 1.b***. The friction between the yarn and yarn guide of the PM ring was measured with a CTT (constant tension transport) friction tester and was used for simulation of the model.

Numerical solution of the theoretical model

The ***Equation (6)*** is a 2nd order differential equation of the dynamic yarn path considering the BCR and yarn elasticity. The components of ***Equations (8)-(10)*** are integrated with the Runge-Kutta method with a spatial step size of 0.0001 using the MATLAB program and are further optimised using the shooting method so that the above-mentioned boundary conditions in (***Equations (11)-(14)***) are fulfilled. Finally an iterative optimisation method: 'Levenberg-Marquardt algorithm' has been applied to minimise the squared error residual sum of the reformulated boundary conditions. The algorithm minimises the non-linear least square problem to establish the local minimum and satisfy the convergence criteria of the algorithm. The solution of ***Equations (8)-(10)***, due to their high non-linearity, is strongly dependent on

$$m\{\mathfrak{D}^2 R + 2\omega_{PM} e_z \times \mathfrak{D}R + \omega_{PM}^2 e_z \times (e_z \times R)\} = \frac{\partial}{\partial s}\left(T.\frac{1}{(1+\varepsilon)} \cdot \frac{\partial R}{\partial s}\right) + F + F_c \tag{6}$$

$$F = -D_n v_n \boldsymbol{v_n}(1+\varepsilon) \quad \text{with} \quad D_n = \frac{1}{2}\rho d c_d \quad \text{and} \quad d = \sqrt{\frac{\pi m}{\rho_m}} \tag{7}$$

$$\frac{1}{(1+\varepsilon)}\left(T_0 - \frac{1}{2}m\omega^2 r^2\right)\left(r'' - r\theta'^2\right) = \omega^2\left(\frac{1}{(1+\varepsilon)^2} \cdot mrr'^2 - mr - \frac{1}{2}\rho d c_d \cdot \frac{1}{(1+\varepsilon)^2} \cdot r^3\sqrt{r'^2 + z'^2}\, r'\theta'\right) - F_r \tag{8}$$

$$\frac{1}{(1+\varepsilon)}\left(T_0 - \frac{1}{2}m\omega^2 r^2\right)(r\theta'' + 2r'\theta') = \frac{\omega^2}{(1+\varepsilon)^2}(mr^2 r'\theta' + \frac{1}{2}\rho d c_d \cdot r^2\sqrt{r'^2 + z'^2})^3 + \mu_c\left(\sqrt{F_r^2 + F_z^2}\right) \tag{9}$$

$$\frac{1}{(1+\varepsilon)}\left(T_0 - \frac{1}{2}m\omega^2 r^2\right)z'' = \frac{\omega^2}{(1+\varepsilon)^2}(mrr'z' - \frac{1}{2}\rho d c_d \cdot r^3\sqrt{r'^2 + z'^2} \cdot \theta' z') - F_z \tag{10}$$

Equations (6), (7), (8), (9) and (10).

the initial values. Hence a sensitivity analysis in terms of the initial values is necessary to find an optimal solution with the above- mentioned iterative optimisation algorithm [13]. The minimisation of the residual error for a set of initial trial values T_0 and $r'(0)$ is calculated from the sensitivity analysis, which delivers an optimal set of trial values which fulfil the boundary conditions.

For the numerical solution, boundary conditions (***Eqations (11)-(14)***) are considered. The yarn path from the delivery rollers up to the winding point of the cop is assumed to be continuous at the BCR. In comparison to the numerical solution of the free balloon, the balloon form has been calculated in two steps. In the first, the equation of motion has been integrated using the shooting method to solve the balloon form between the yarn guide and BCR considering the boundary conditions (***Eqations (11)-(12)***). The results i.e. the yarn tension and coordinate system, determine the initial values of yarn tension at the yarn guide T_0 and the gradient of the balloon form. In the 2nd step, the balloon form between the BCR and PM ring has been predicted considering the boundary conditions from ***Eqations (13)-(14)***. Both solutions should satisfy the conditions for geometrical continuity of the thread line at the BCR and also the boundary conditions at the guide eye and PM ring. The input parameters considered for the numerical solution and for the experiments are listed in ***Table 1***. As a result of the numerical solution, the yarn tension in regions I-IV and the balloon form considering the balloon control ring and yarn elasticity are determined with respect to different angular spindle speeds.

Results and discussion

In ***Figure 2*** the yarn tensions predicted in region I-IV have been illustrated considering the balloon control ring and yarn elasticity with respect to angular spindle speeds from 5.000-50.000 r.p.m.

Yarn tensions increase in all regions along with the angular spindle speed. The highest tension occurs in region IV for a certain spindle speed.

The corresponding geometry of the balloon have been presented in relation to the different spindle speeds, from 5.000-50.000 r.p.m. (***Figure 3***). The balloon forms also increase due to the centrifugal forces with respect to different angular spindle speeds from 5.000 to 50.000, as shown in ***Figure 3***. According to ***Figure 3***, the yarn balloon changes to a little extent in the range of angular spindle speed 30.000-50.000 r.p.m. The yarn elasticity behaviour at such a higher tension and angular spindle speed does not follow the linear elasticity rules.

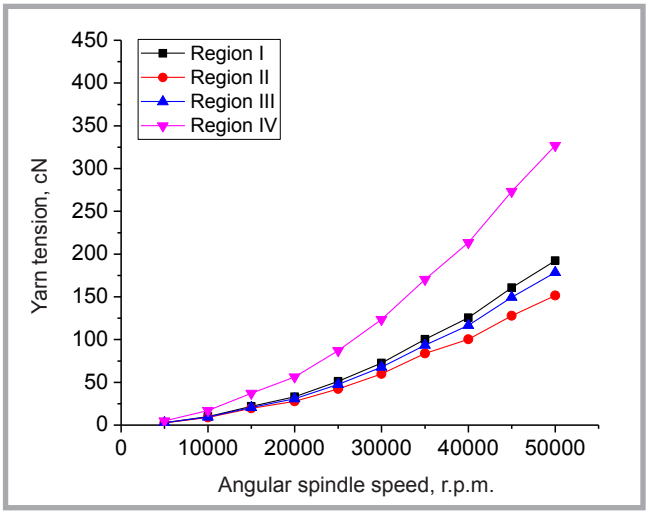

Figure 2. *Prediction of yarn tension considering the balloon control ring and yarn elasticity with respect to different angular spindle speeds in the SMB ring spinning process. Region I: between the delivery rollers and yarn guide; Region II: between the yarn guide and PM ring: Region III: through the guide at the PM ring: Region IV: between the yarn guide at the PM ring and the winding point of the cop.*

In order to understand the influence of the BCR and yarn elasticity, the yarn tensions in regions I and IV have been compared with and without considering the balloon control ring and yarn elasticity. As shown in ***Figure 4***, the yarn tension considering the BCR and yarn elasticity is 10% less than that not considering the BCR at an angular spindle speed of 50.000 r.p.m.

Characterisation of dynamic yarn path

In order to characterise the dynamic yarn path in the model presented, the yarn tensions were measured in regions I and II. Moreover the balloon forms were recorded with a high speed camera considering the balloon control ring.

Yarn tension between delivery rollers and yarn guide (Region I)

A modified 3-point sensor from Tensometric Messtechnik GmbH was used for the measurement of tension in region I at different angular spindle speeds from 5.000-15.000 r.p.m. (***Figure 5.a***). In order to measure the yarn tension, the sensor was modified by replacing the guiding and measuring elements with rotating rollers. Thus the twist could further propagate from the SMB twisting system to the delivery rollers without causing any end-breakages.

During calibration, dead weights of 10 g and 20 g are hung over with spun yarn to set the scale in the data acquisition program. The experiment is repeated to verify the values measured for a constant angular spindle speeds. Mean values of yarn tension for different spindle speeds were recorded with a LabView Signal Express.

Table 1. *Process parameters considered for the numerical solution and experiments.*

Parameter	Value	Unit
Material	100% cotton	
Staple length	28	mm
Roving count	565	tex, g/km
Yarn count, m	20	tex, g/km
Spindle speed, n_s	5000, 10000, 15000	rpm
Delivery speed, v	7.1, 14.3, 21.4	m/min
Twist	700	T/m
Balloon height, h	180	mm
Diameter of balloon control ring	44	mm
Friction between yarn and yarn guide of PM ring, μ_y	5000; 10000; 15000 (0.21; 0.23; 0.24) 30000; 40000; 50000 (0.26; 0.26; 0.27)	
Mass of PM ring, m_{PM}	241±1	g
Inner diameter of PM ring, a_{iPM}	43	mm
Outer diameter of PM ring, a_{aPM}	80	mm

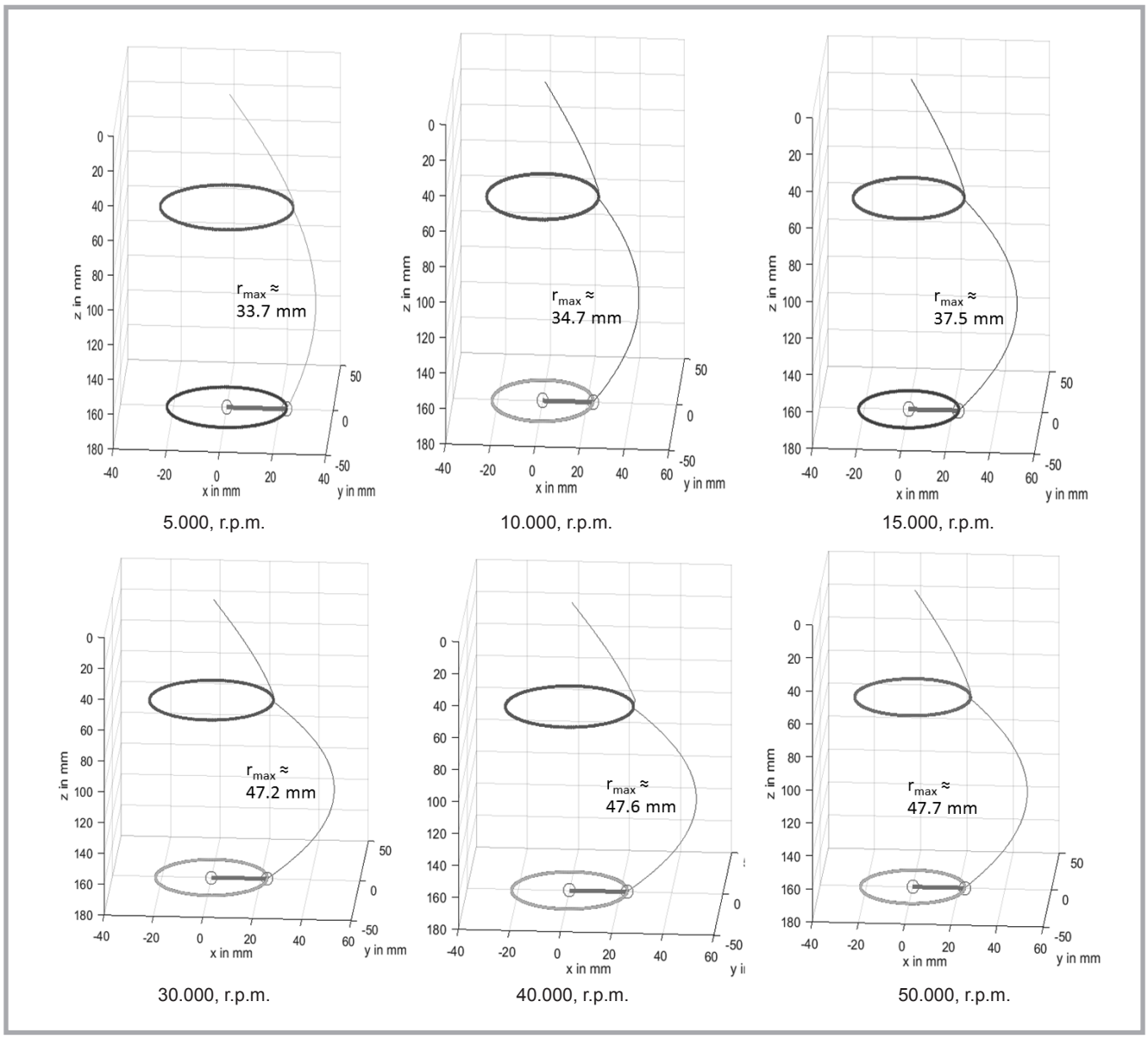

Figure 3. *Calculated balloon forms with respect to angular spindle speeds from 5.000-50.000 r.p.m.*

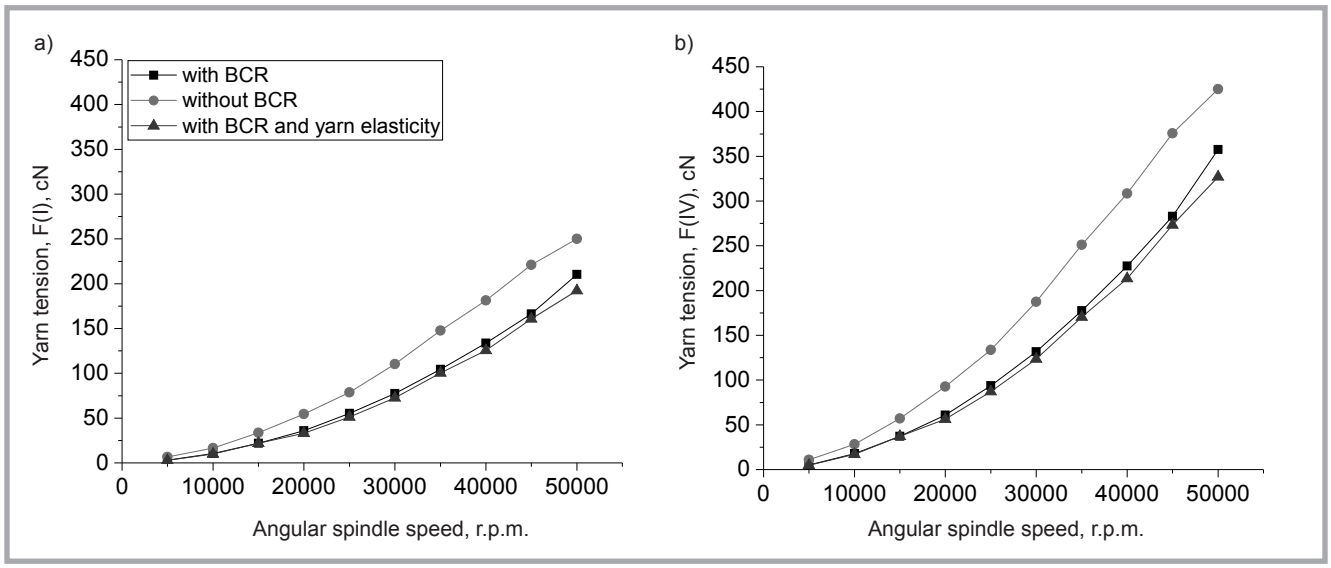

Figure 4. *Comparison of yarn tension considering the BCR, without the BCR and yarn elasticity with respect to different angular spindle speeds in a) region I and b) IV.*

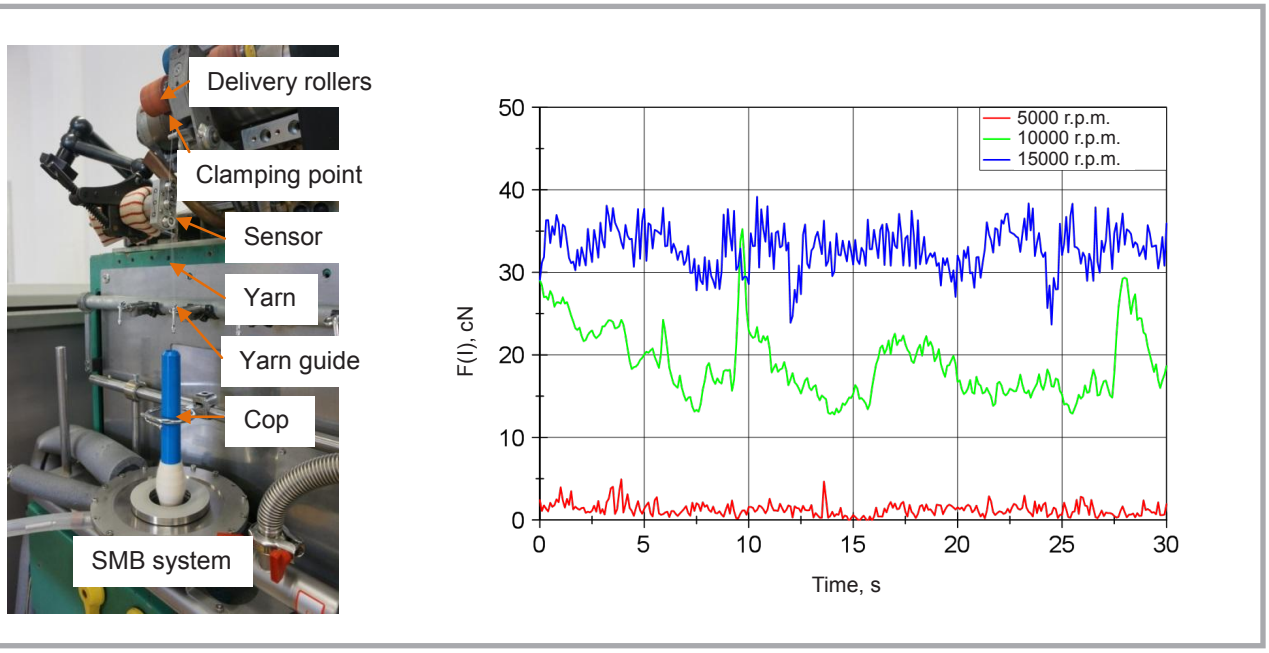

Figure 5. *a) Measurement set-up for yarn tension in region I between delivery rollers and yarn guide and b) mean values of yarn tension in region I at different spindle speeds.*

According to ***Figure 5.b***, the yarn tension increases with a higher angular spindle speed. As the spindle speed increases (such as to 15.000 r.p.m.), the vibration of the PM ring and movement of the ring rail cause yarn tension variation.

Balloon form (Region II)

The balloon forms were recorded with a high speed camera (Photron Fastcam Ultima SA-3, frame rate 12.5 KHz for 1024×1024 Pixel) at different spindle speeds from 5.000 to 15.000 r.p.m. with the built-in balloon control ring (***Figure 6***). The recording of balloon forms was carried out on an SMB ring spinning tester to find out the influence of the balloon control ring on the balloon form.

At a higher spindle speed, the maximum radius of the balloon locates in the middle of the balloon control ring and PM ring due to the higher centrifugal force (***Figure 7***). Images of the balloon form recorded were analysed to measure the maximum balloon diameter using Image J software. Each maximum balloon form for a defined spindle speed was measured several times with this program.

Yarn tension between yarn guide and PM ring (Region II)

Measurement of yarn tension in region II was conducted with the SMB system from the balloon forms recorded with the high speed camera. In this case, a method of measuring the deformation of yarn from the balloon forms recorded was used [16]. In the first step, the deformation behaviour (strain %) of the yarn was measured from the balloon form recorded using digital image analysis software. In the second step, the spun yarn was tested to determine the stress-strain curve. Finally the yarn tension was calculated comparing the deformation of yarn in the balloon measured with that from the stress-strain diagram tested.

Figure 8 shows the measurement of yarn deformation at different positions of the balloon form using contrast fibers at an angular spindle speed of 10.000 r.p.m.

The corresponding stress-strain diagram from the same spun yarn measured with a tensile testing machine – Uster Tensorapid 3 is shown in ***Figure 9.a***.

Thus the yarn deformation measured (strain %) from the balloon form record-

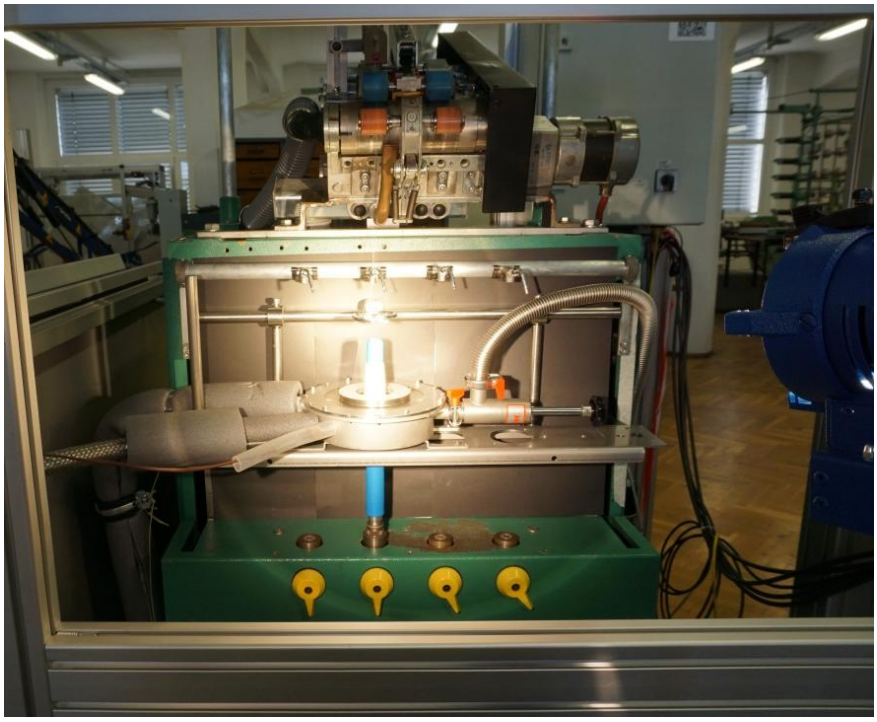

Figure 6. *Recording the balloon form with a high speed camera on an SMB ring spinning tester considering the balloon control ring.*

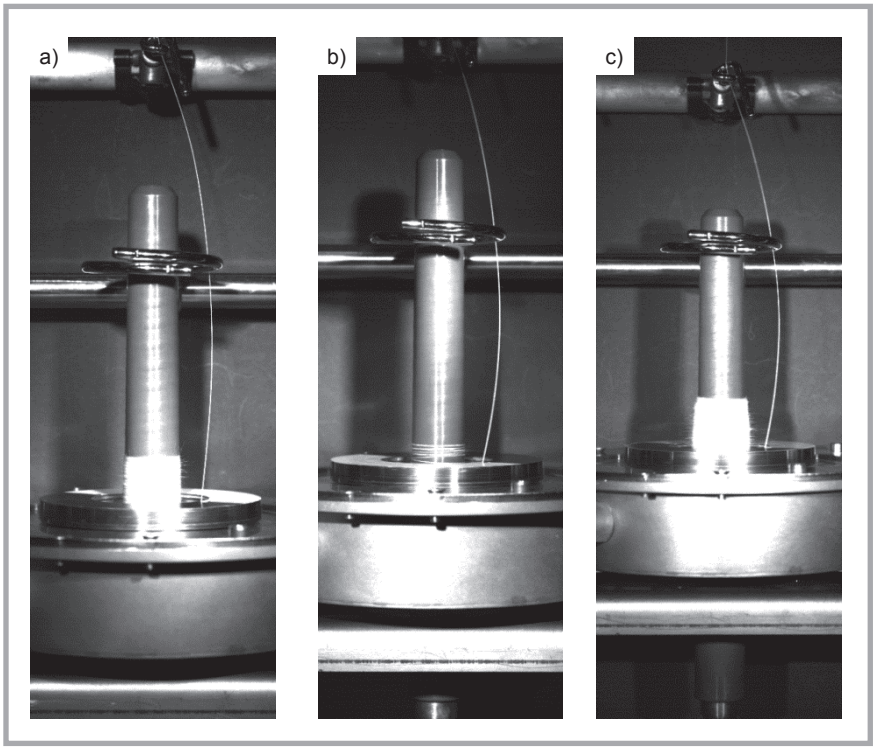

Figure 7. *Balloon forms recorded with a high speed camera with respect to different angular spindle speeds of 5.000-15.000 rpm considering the balloon control ring: a) 5.000 r.p.m., b) 10.000 r.p.m., b) 15.000 r.p.m.*

Table 2. *Comparison between the max. balloon diameter and that calculated and measured.*

Spindle speed, r.p.m.	Max. balloon diameter calculated, mm	Max. balloon diameter measured, mm	Absolute error, mm
5000	67.4	43.42	23.98
10000	69.4	46.64	22.76
15000	75	50.88	24.12

ed is considered to determine the corresponding values of yarn tension from the stress-strain diagram (***Figure 9.b***).

Validation of the model developed

For validation of the yarn tension values calculated in regions I and II as well as the corresponding balloon forms, they are compared to the measured ones at angular spindle speeds from 5.000 to 15.000 r.p.m. ***Figure 10*** illustrates the results for yarn tension measured with the sensor compared to the calculated ones at different angular spindle speeds. It is clear that the simulated values display good correlation with the values measured and confirm the prediction of yarn tensions at different angular spindle speeds.

However, the experimentally determined yarn tensions are generally higher than the calculated ones, especially at higher angular spindle speeds, such as 15.000 r.p.m., because some factors such as the vibration of the PM ring during the spinning process and the resulting vibration of the yarn are not considered in the mathematical modelling. The difference between the calculated and measured yarn tensions might be increased due to the vibration of the PM for all regions, especially at higher angular spindle speeds.

The calculated balloon forms (from ***Figure 4***) and measured ones (from

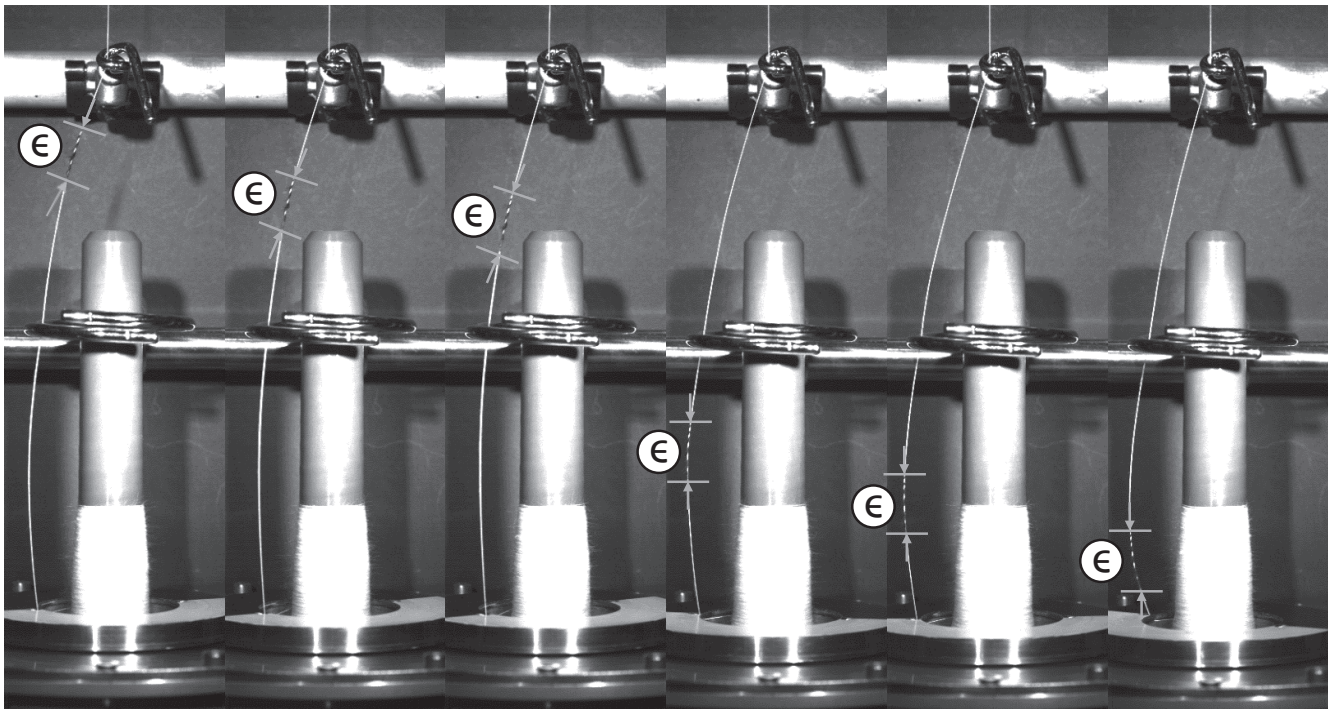

Figure 8. *Measurement of deformation behaviour of yarn i.e. strain, % (ϵ) from balloon form recorded at an angular spindle speed of 10.000 r.p.m*

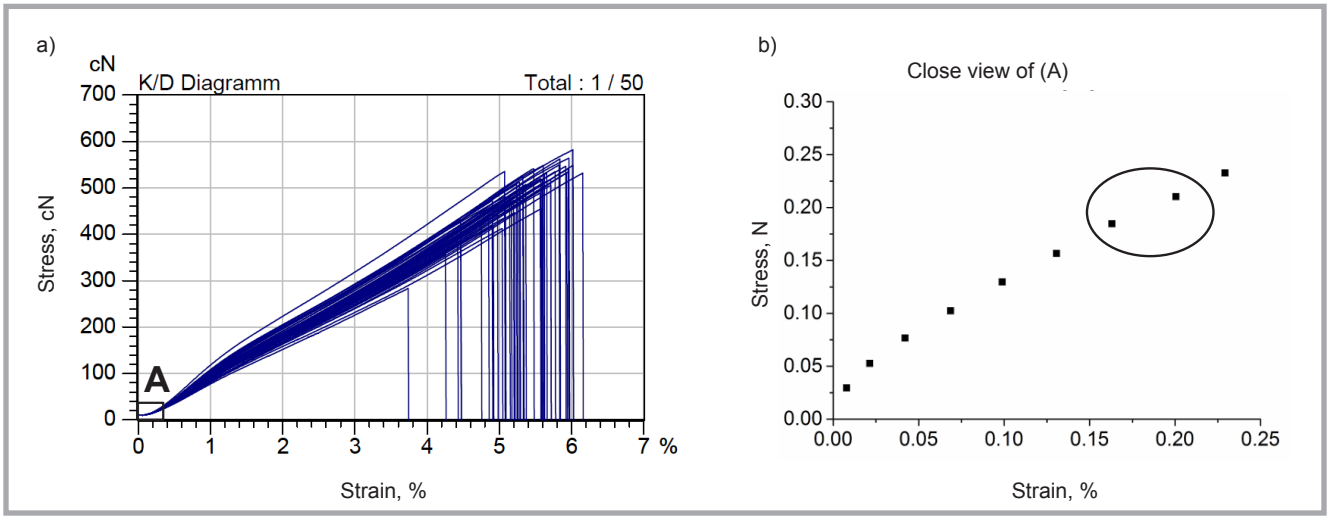

Figure 9. *a) Stress-strain diagram of spun yarn, b) yarn tension calculated by comparing the yarn strain measured from the balloon form with that from the stress-strain diagram at an angular spindle speed of 10.000 r.p.m.*

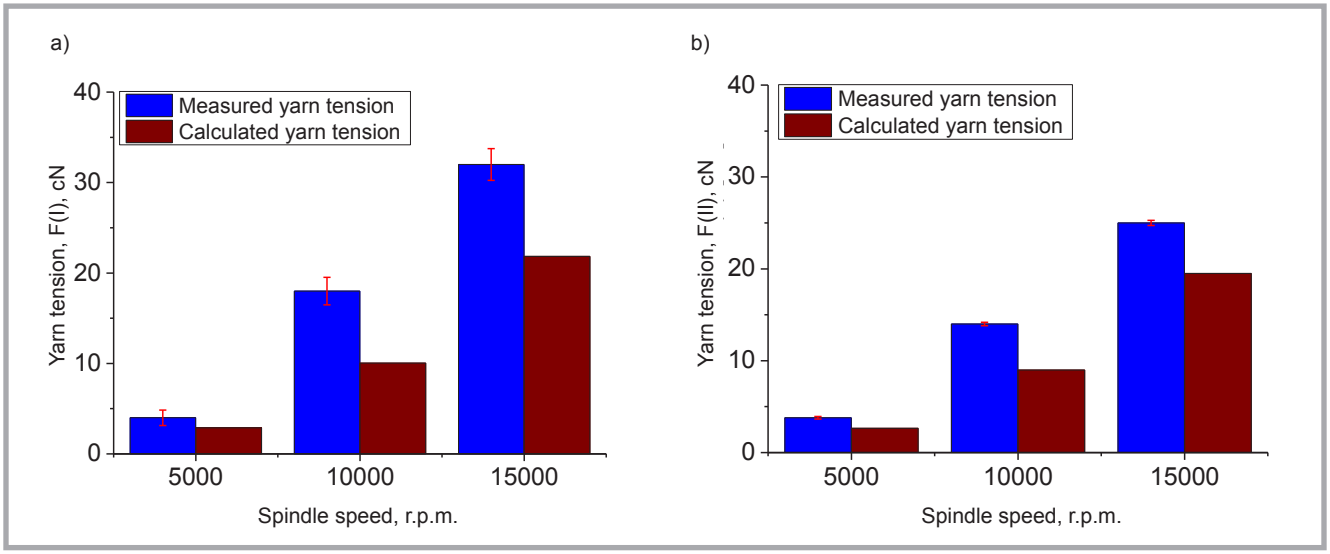

Figure 10. *Comparison of measured and calculated yarn tension values for (a) region I – delivery roller to yarn guide and b) region II – yarn guide to permanent magnet ring.*

Figure 7) can be compared with regard to angular spindle speeds from 5.000 to 15.000 r.p.m.,which shows a good correlation between the calculated and measured balloon forms.

Moreover the maximum values of the balloon diameters are quantitatively compared in ***Table 2*** for different spindle speeds.

The errors in ***Table 2*** can be attributed to the numerical solution method in the model presented. In this model, the balloon form has been calculated in two steps considering the balloon between the yarn guide and BCR (1st balloon) as well as between the BCR and PM ring (2nd balloon). In the numerical calculation for the 2nd balloon, the initial values such as the yarn tension and slope of the 1st balloon at the balloon control ring are considered to calculate the 2nd balloon. Thus regarding the BCR, the balloon is bigger than that without the balloon control ring. However, the aim of using the balloon control ring is to decrease the balloon form, which can be seen from the balloon form recorded, shown in ***Figure 7***.

Conclusions and outlook

The friction free SMB system eliminates the frictional problem of the existing ring/traveler system in the ring spinning process. However, the yarn tension increases with respect to the angular spindle speed due to the centrifugal force of the rotating balloon. The balloon control ring reduces the yarn tension by dividing the component of yarn tension in the rotating balloon. In this paper, a theoretical model of the dynamic yarn path has been established for a quasi-stationary case considering the balloon control ring and yarn elasticity in the SMB ring spinning process. As the solution of the equations are extremely nonlinear, a sensitivity analysis was conducted to find a valid set of initial values which fulfil the boundary conditions. The 2nd order differential equations were integrated with the Runge-Kutta method using the MATLAB program. The residual error of the numerical solution was further optimised with the 'Levenberg-Marquardt algorithm', which satisfies the convergence criteria for the valid initial values. According to the numerical results, the yarn tension increases along with the increased angular spindle speeds. The yarn tension when using a BCR in the SMB ring spinning process decreases

by a minimum of 10% compared to that without the BCR.

The elasticity of yarn also reduces the yarn tension to some extent, which has been shown from the model presented. According to the model developed, the balloon form increases with respect to different angular spindle speeds. This increment is dominant up to an angular spindle speed of 25.000 r.p.m. At an angular spindle speed of 30.000 to 50.000 r.p.m., the balloon form increases to a certain amount. At such a high spindle speed, the yarn tension is so great that the yarn does not follow the rules of linear elasticity i.e. Hooke's law. Hence the non-linear behaviour of the yarn has to be considered in future work. The influence of elasticity can be further analysed using the nonlinear elastic constitutive law. The stress-strain curves can be further investigated, which are nonlinear. Moreover a high speed camera is used to record balloon forms considering the balloon control ring with respect to an angular spindle speed from 5.000-15.000 r.p.m. in order to validate the model developed. The model will be validated after modification of the existing SMB ring spinning machine to be compatible to an angular spindle speed up to 50.000 r.p.m. In this case, the friction between the yarn and yarn guiding elements (such as BCR) has to be considered, as it influences the spinning process, especially for thermoplastic materials.

Funding

This research is funded by the German Research Foundation, DFG (Project No. CH 174/33-2 and SCHU 1118/12-2). The authors would like to thank DFG for the financial support.

References

1. DE 11 2012 000 596 A5. evico GmbH Dresden; Leibniz-Institut für Festkörper-und Werkstoffforschung Dresden e.V.; Technische Universität Dresden. (16.01.2014). Cherif, Ch.; Abdkader, A.; Schultz, L., *et al*.
2. Hossain M, Abdkader A, Cherif Ch, *et al*. Innovative twisting mechanism based on superconducting technology for higher productivity in ring spinning machine. Textile *Research Journal* 2014; 84, 8: 871-880.
3. Sparing M, Berger A, Hossain M, Berger D, Fuchs G. Abdkader A, Cherif Ch, Schultz L. Dynamics of rotating superconducting magnetic bearings in ring spinning. *IEEE Transactions on Applied Superconductivity* 2016; 26, 3: 3600804.
4. Berger A, Sparing M, Hossain M, Berger D, Fuchs G, Abdkader A, Cherif C, Schultz L. Cryogenic System for the Integration of a RingShaped SMB in a Ring-Spinning Tester. IEEE Transactions on Applied Superconductivity 26(2016)3, pp. 3601105/1-5.
5. Sparing, M, Hossain M, Berger D, Berger A, Abdkader A, Fuchs G, Cherif C, Schultz L. Superconducting magnetic bearing as twist element in textile machines, IEEE Transactions on Applied Superconductivity 25(2015)3, pp. 3600504.
6. Batra S K, Ghosh TK, Zeidman MI. An Integrated Approach to Dynamic Analysis of the Ring Spinning Process: Part I: Without Air Drag and Coriolis Acceleration. *Textile Research Journal* 1989; 59, 6: 309-317.
7. Batra SK, Ghosh TK, Zeidman MI. An Integrated Approach to Dynamic Analysis of the Ring Spinning Process, Part II: With Air Drag and Coriolis Acceleration. *Textile Research Journal* 1989; 59, 7: 416-424.
8. Ghosh TK, Batra SK, Zeidman MI, *et al*. An Integrated Approach to Dynamic Analysis of the Ring Spinning Process, Part III: The Effect of Coefficient of Friction and the Balloon Control Rings. *Textile Praxis International* 1992; 47: 791-800.
9. Batra SK, Ghosh TK, Fraser WB, *et al*. An Integrated Approach to Dynamic Analysis of the Ring Spinning Process, Part IV: Inherent Instability of the Free Balloon. *Textile Research Journal* 1995; 65, 7: 417-423.
10. Fraser WB. On the Theory of Ring spinning. *Philosophical Transactions of the Royal Society of London A: Mathematical, Physical and Engineering Sciences* 1993; 342, 1665: 439-468.
11. Fraser WB. The effect of a control ring on the stability of the ring-spinning balloon. *Philosophical Transactions of the Royal Society of London A: Mathematical, Physical and Engineering Sciences* 1996; 47, 452: 47-62.
12. Tang ZX, Fraser WB, Wang L, Wang X. Examining the effects of balloon control ring on ring spinning. *Fibers and Polymers* 2008; 9,5: 625-632.
13. Hossain M, Telke C, Abdkader A, Cherif Ch, Beitelschmidt M. Mathematical modelling of the dynamic yarn path depending on spindle speed in a ring spinning process. *Textile Research Journal* 2015; 86, 11: 1180-1190.
14. Hossain M, Telke C, Sparing M, Abdkader A, Cherif Ch, Beitelschmidt M, Schultz L. Mathematical modelling of the dynamic yarn path depending on spindle speed in a ring spinning process based on superconducting magnetic bearing. *Textile Research Journal* 2016; 86, 11: 1180-1190.
15. Yin R, Gu HB. Numerical simulation of quasi-stationary ring spinning process linear elastic yarn. *Textile Research Journal* 2011; 81, 1: 22-27.
16. Hossain M, Abdkader A, Cherif Ch, *et al*. Measurement methods of dynamic yarn tension in a ring spinning process. *FIBRES & TEXTILES in Eastern Europe* 2016; 24, 1(115): 36-43. DOI: 10.5604/12303666.1172098.

Received 18.04.2018 Reviewed 06.06.2018